



Geometry of charged rotating discs of dust in Einstein-Maxwell theory

David Rumler¹ · Andreas Kleinwächter¹ · Reinhard Meinel¹

Received: 11 November 2022 / Accepted: 29 January 2023 / Published online: 7 February 2023
© The Author(s) 2023

Abstract

Within the framework of Einstein-Maxwell theory geometric properties of charged rotating discs of dust, using a post-Newtonian expansion up to tenth order, are discussed. Investigating the disc's proper radius and the proper circumference allows us to address questions related to the Ehrenfest paradox. In the Newtonian limit there is an agreement with a rotating disc from special relativity. The charged rotating disc of dust also possesses material-like properties. A fundamental geometric property of the disc is its Gaussian curvature. The result obtained for the charged rotating disc of dust is checked by additionally calculating the Gaussian curvature of the analytic limiting cases (charged rotating) Maclaurin disc, electrically counterpoised dust-disc and uncharged rotating disc of dust. We find that by increasing the disc's specific charge there occurs a transition from negative to positive curvature.

Keywords Charged rotating disc of dust · Post-Newtonian expansion · Ehrenfest paradox · Gaussian curvature · Maclaurin disc · Electrically counterpoised dust

Contents

| | | |
|-----|--|----|
| 1 | Introduction | 2 |
| 2 | Boundary value problem for the charged disc of dust | 3 |
| 3 | Post-Newtonian expansion | 5 |
| 4 | Related questions to Ehrenfest's paradox | 6 |
| 5 | Curvature | 12 |
| 5.1 | Gaussian curvature of the charged disc of dust | 12 |
| 5.2 | Newtonian theory: Maclaurin discs and their Gaussian curvature | 14 |
| 5.3 | Gaussian curvature of a specific ECD-disc configuration | 16 |
| 5.4 | Gaussian curvature of the uncharged disc of dust | 19 |
| 5.5 | Visualization | 21 |
| 5.6 | Transition curve | 22 |

✉ David Rumler
david.rumler@uni-jena.de

¹ Theoretisch-Physikalisches Institut, Friedrich-Schiller-Universität Jena, Max-Wien-Platz 1, 07743 Jena, Germany

| | |
|---|----|
| 6 Discussion | 22 |
| Appendix A Expansions up to fifth order | 24 |
| Appendix B Gaussian curvature | 25 |
| References | 25 |

1 Introduction

In 1909 Ehrenfest formulated a famous paradox concerning a rigidly rotating disc (or a cylinder in the original version) within special relativity [1]. He pointed out that special relativistic rigidity, introduced by Born [2], easily leads to two contradicting statements about radius and circumference measured by a non-rotating observer before and after the disc is set into rotation.

The paradox gave rise to a long lasting debate on how to resolve it, see, e.g., [3]. Numerous physicists came up with solution approaches, however, they turned out to be wrong in most cases. Grøn presented in 1975 a resolution solely based on kinematics [4]. Initially, it was not clear whether this would be sufficient or whether a dynamical treatment would be necessary to solve the problem completely. Today, most physicists (including the authors of this paper) accept Grøn's kinematic considerations as the correct way to resolve Ehrenfest's paradox.

Nevertheless there are related questions to the paradox, as how the ratio of circumference to radius is observed from the point of view of non-rotating versus co-rotating observers (on the disc), how those measurements change when the rotation speed is altered and how material properties affect more realistic discs.

With the help of the available semi-analytic solution of the charged rotating disc of dust, which is a concrete, physically relevant solution of the Einstein-Maxwell equations in terms of a post-Newtonian expansion [5], we can tackle the above questions in a very direct way.

Motivated by those geometric investigations it is also natural to ask about the intrinsic curvature of the charged rotating disc of dust. For a two-dimensional disc the intrinsic curvature is simply the Gaussian curvature. In particular, the post-Newtonian expansion allows us not only to study special relativistic effects, but also investigate the influence of higher order corrections coming from general relativity. A key observation is that the specific charge of the disc acts like a regulator to adjust the curvature of the disc. More precisely, by increasing the specific charge from 0 to 1 there is a critical value at which a transitions from negative to positive curvature occurs.

The present paper is structured as follows. In Sect. 2 we briefly introduce the mathematical formulation of the disc problem in terms of a boundary value problem, followed by a short overview of the used post-Newtonian expansion in Sect. 3. After defining the proper radius and the proper circumference of the rotating disc in Sect. 4, we discuss the above mentioned questions related to the Ehrenfest paradox based on the charged rotating disc of dust. Sect. 5 is devoted to the curvature of the disc. The result will be compared with the ones for a Maclaurin disc within Newtonian theory, a disc with a concrete electrically counterpoised dust-configuration (having maximal charge) and the uncharged disc of dust.

2 Boundary value problem for the charged disc of dust

We consider an equilibrium configuration of an infinitesimally thin disc of dust (perfect fluid with vanishing pressure) with constant specific charge $\epsilon = \frac{\rho_{el}}{\mu} \in [-1, 1]$ and constant angular velocity Ω [5–7]. ρ_{el} and μ denote the charge density and the baryonic mass density of the disc, respectively.

The corresponding disc problem is formulated in the framework of Einstein-Maxwell equations¹:

$$R_{ab} - \frac{1}{2}R g_{ab} = 8\pi T_{ab} , \tag{1}$$

$$F^{ab}{}_{;b} = 4\pi j^a , \tag{2}$$

where

$$T_{ab} = T_{ab}^{(em)} + T_{ab}^{(dust)} = \frac{1}{4\pi} \left(F_{ac} F_b{}^c - \frac{1}{4} g_{ab} F_{cd} F^{cd} \right) + \mu u_a u_b , \tag{3}$$

$$j^a = \rho_{el} u^a = \epsilon \mu u^a , \tag{4}$$

$$F_{ab} = A_{b;a} - A_{a;b} = A_{b,a} - A_{a,b} . \tag{5}$$

To the energy momentum tensor, T_{ab} , both the electromagnetic field and matter (dust) contribute. j^a represents a purely convective four-current density, where u^a is the four-velocity. As is common practice, the field strength tensor F_{ab} is expressed in terms of the four-potential A_a .

For an equilibrium configuration, spacetime is stationary, implying the existence of an associated Killing vector ξ . We also demand axisymmetry, characterized by another Killing vector η that commutes with ξ . Furthermore, the problem is reflection symmetric with respect to the equatorial plane of the disc.

Exploiting stationarity and axisymmetry the line element can globally be written in terms of Weyl-Lewis-Papapetrou coordinates:

$$ds^2 = f^{-1} \left[h \left(d\rho^2 + d\zeta^2 \right) + \rho^2 d\varphi^2 \right] - f \left(dt + a d\varphi \right)^2 . \tag{6}$$

Using Lorenz-gauge the four-potential A_a takes the form:

$$A_a = (0, 0, A_\varphi, A_t) . \tag{7}$$

The coordinates t and φ used in the line element are adapted to the Killing vectors, such that

$$\xi = \frac{\partial}{\partial t} \quad \text{and} \quad \eta = \frac{\partial}{\partial \varphi} . \tag{8}$$

As a consequence, the metric functions f , h , and a as well as the potentials A_φ and A_t depend on the coordinates ρ and ζ only. Instead of f and h we will also make use of the functions U and k , where $f = e^{2U}$ and $h = e^{2k}$.

¹ We use units in which $c = G = 4\pi\epsilon_0 = 1$.

In the subsequent discussion we heavily rely on the co-rotating frame of reference defined by $\varphi' = \varphi - \Omega t$. As usual, the covariance of the metric and the four-potential imply the following transformation laws:

$$f' = f \left[(1 + \Omega a)^2 - \Omega^2 \rho^2 f^{-2} \right], \quad (1 - \Omega a') f' = (1 + \Omega a) f, \quad \frac{h'}{f'} = \frac{h}{f}, \tag{9}$$

$$A'_{\varphi'} = A_\varphi, \quad A'_t = \Omega A_\varphi + A_t. \tag{10}$$

It should be noted that the mass density μ is related to the surface mass density σ via

$$\mu = \frac{f}{h} \sigma(\rho) \delta(\zeta). \tag{11}$$

However, σ is not coordinate independent in contrast to the proper surface mass density

$$\sigma_p = \sqrt{\frac{f}{h}} \sigma. \tag{12}$$

In (electro-)vacuum, assuming axisymmetry and stationarity, the combined Einstein-Maxwell equations in terms of f, h, a, A_φ and A_t , that can be found in [6], can be reduced to the Ernst equations [8]:

$$\left(\Re \mathcal{E} + |\Phi|^2 \right) \Delta \mathcal{E} = (\nabla \mathcal{E} + 2\bar{\Phi} \nabla \Phi) \cdot \nabla \mathcal{E}, \tag{13}$$

$$\left(\Re \mathcal{E} + |\Phi|^2 \right) \Delta \Phi = (\nabla \mathcal{E} + 2\bar{\Phi} \nabla \Phi) \cdot \nabla \Phi, \tag{14}$$

where

$$\Phi = \alpha + i\beta \quad \text{and} \quad \mathcal{E} = (f - |\Phi|^2) + ib, \tag{15}$$

with $\alpha := \Re \Phi = -A_t$, are the Ernst potentials. The potentials β and b are defined via

$$\beta_{,\rho} = \frac{f}{\rho} (A_{\varphi,\zeta} - a A_{t,\zeta}), \quad \beta_{,\zeta} = -\frac{f}{\rho} (A_{\varphi,\rho} - a A_{t,\rho}) \tag{16}$$

and

$$b_{,\rho} = -\frac{f^2}{\rho} a_{,\zeta} - 2(\beta A_{t,\rho} - A_t \beta_{,\rho}), \quad b_{,\zeta} = \frac{f^2}{\rho} a_{,\rho} - 2(\beta A_{t,\zeta} - A_t \beta_{,\zeta}). \tag{17}$$

∇ and Δ are meant as operators in 3-dimensional Euclidean space with cylindrical coordinates ρ, ζ and φ . Note that the integrability conditions for (16) and (17) are automatically satisfied as a consequence of the Einstein-Maxwell equations. Vice versa, (16) and (17) may be used to obtain a and A_φ from the solutions to the Ernst equations by a path-independent line integration. The function h can be determined by a path-independent line integration from the other functions as well.

Using reflection symmetry the following boundary conditions on the disc, i.e. for $0 \leq \rho \leq \rho_0$ and $\zeta = 0$, where ρ_0 is the coordinate radius, can be derived:

$$b' = 0, \quad \beta' = 0, \quad (e^{U'} - \epsilon A'_t)_{,\rho} = 0, \quad (A'_t - \epsilon e^{U'})_{,\zeta} = 0. \tag{18}$$

The Ernst equations (13) and (14) together with the boundary conditions (18), as well as the asymptotic flatness condition ($\mathcal{E} \rightarrow 1$ and $\Phi \rightarrow 0$ for $\rho^2 + \zeta^2 \rightarrow \infty$) and the regularity condition at the rim of the disc, form a well-defined boundary value problem for the charged disc of dust.

3 Post-Newtonian expansion

In case of the rotating disc of dust without charge the corresponding boundary value problem could be solved analytically [9, 10]. For the charged rotating disc of dust a semi-analytic solution in terms of a post-Newtonian expansion up to tenth order is available [5, 6].

This expansion uses a relativity parameter γ [11], defined by

$$\gamma := 1 - \sqrt{f_c}, \quad \text{with } f_c := f(\rho = 0, \zeta = 0). \tag{19}$$

Equivalently, γ can be expressed in terms of the redshift, Z_c , of a photon emitted at $\rho = 0, \zeta = 0$ and observed at $\rho^2 + \zeta^2 \rightarrow \infty$:

$$\gamma = \frac{Z_c}{1 + Z_c}. \tag{20}$$

From both expressions, (19) and (20), it is evident that γ takes values between 0 and 1, where $\gamma \approx 0$ represents Minkowski spacetime and $\gamma \rightarrow 1$ corresponds to the ultra-relativistic limit. At the ultra-relativistic limit we assume the formation of black holes [5]. Note that U , appearing in $f_c = e^{2U_c}$, can be interpreted as a generalized Newtonian potential.

The parameter space of the charged disc solution is spanned by $\gamma \in [0, 1], \epsilon \in [0, 1]$ and the coordinate radius ρ_0 as a scaling parameter. By restricting to positive charges we do not lose generality.²

A convenient choice of coordinates is given in terms of elliptic coordinates η and ν , defined through

$$\rho = \rho_0 \sqrt{(1 - \eta^2)(1 + \nu^2)}, \quad \zeta = \rho_0 \eta \nu, \tag{21}$$

with $\eta \in [-1, 1]$ and $\nu \in [0, \infty]$. Additionally normalizing all dimensioned quantities with suitable powers of ρ_0 leads to a dimensionless formulation of the disc problem.

² In fact, all dimensionless physical parameters describing the disc are functions of γ and ϵ , in particular $\rho_0 \Omega, M/\rho_0$ and J/ρ_0^2 (with M and J being gravitational mass and angular momentum).

The normalized quantities are denoted by $*$, e.g.

$$a^* = \frac{a}{\rho_0}, \quad A_\varphi^* = \frac{A_\varphi}{\rho_0} \quad \text{or} \quad \Omega^* = \rho_0 \Omega. \tag{22}$$

As a starting point of the post-Newtonian expansion we utilize the relation

$$\gamma = -U_N(\rho = 0, \zeta = 0) = \frac{\Omega_N^{*2}}{1 - \epsilon^2}, \tag{23}$$

between the Newtonian potential U_N and the angular frequency Ω_N that holds in Newtonian limit only. As a consequence, we have $\Omega^{*2} = (1 - \epsilon^2)\gamma + \mathcal{O}(\gamma^2)$ in general (beyond the Newtonian limit). Expanding this relation implies that Ω^* is an odd function in $g := \sqrt{\gamma}$, i.e.

$$\Omega^* = \sum_{n=0}^{\infty} \Omega_{2n+1}^* g^{2n+1}, \tag{24}$$

where Ω_{2n+1}^* is a function of η and ν and $\Omega_1^* = \sqrt{1 - \epsilon^2}$.³

All the discussed potentials and metric functions can be expanded in Ω^* . Examining their symmetry properties reveals a purely symmetric or antisymmetric behaviour under the transformation $\Omega^* \rightarrow -\Omega^*$ that changes the sense of rotation. Therefore, they can also be written as a series in g , containing only even or odd powers of g , respectively. For the metric functions we get:

$$f = 1 + \sum_{n=1}^{\infty} f_{2n} g^{2n}, \quad h = 1 + \sum_{n=2}^{\infty} h_{2n} g^{2n}, \quad a^* = \sum_{n=1}^{\infty} a_{2n+1}^* g^{2n+1}. \tag{25}$$

All the coefficient functions f_{2n} , h_{2n} and a_{2n+1}^* depend on the coordinates η and ν only.

Palenta and Breithaupt were able to use this post-Newtonian expansion to derive analytic solutions for those coefficient functions. First, Palenta solved the boundary value problem in terms of this expansion up to eighth order ($n = 8$) and Breithaupt later on up to tenth [5, 6]. The subsequent calculations and discussions of the present paper build on Breithaupt’s semi-analytic solution of the charged rotating disc of dust.

4 Related questions to Ehrenfest’s paradox

In 1909 Ehrenfest pointed out that rigid rotation of discs (or cylinders) within special relativity involving a period of angular acceleration inevitably leads to a paradox [1].

³ It turns out that Ω (appropriately normalized, e.g. by R_0 introduced in Sect. 4) increases monotonically with g and decreases monotonically with ϵ . (For both $g = 0$ and $\epsilon = 1$ it vanishes.)

The concept of rigidity in special relativity is defined by Born as follows: Each infinitesimal neighbourhood of an arbitrarily moving body, as measured by co-moving observers at each point of the body, should appear permanently undeformed [2].

Relying on this definition, Ehrenfest formulated a paradox: A relativistic cylinder with radius R is given a rotating motion about its axis, which finally becomes constant - while satisfying Born's rigidity at all times. Let R'' be the radius of the constantly rotating cylinder measured by an observer at rest, then two contradicting requirements need to be fulfilled:

- (i) $2\pi R'' < 2\pi R$,
- (ii) $R'' = R$.

While to this day there is still no common agreement on its solution, there is a kinematic resolution of the paradox by Grøn most physicists do indeed accept [3, 4, 12]. He showed that it is not possible to synchronize clocks of successive inertial rest frames momentarily at rest to points around the periphery of the rotating disc. This means that setting a disc in rotational motion, while satisfying Born's rigidity condition, is kinematically impossible.

Despite its resolution, there are still interesting questions related to Ehrenfest's paradox:

1. How does the spatial geometry of an accelerated disc which is initially at rest evolves as measured by non-rotating and co-rotating observers?
2. What is the spatial geometry of a disc that is already set into rotation as seen by non-rotating and co-rotating observers?
3. A real disc has material properties, how do they influence the rotating disc?

The uniformly rotating disc of dust is relativistically rigid in the sense that it rotates rigidly, meaning $\Omega = \text{const}$. [13].

In the present section we want to describe geometric quantities like proper radius and proper circumference of the rotating disc and address the above posed questions. To this purpose, we introduce the line element

$$d\sigma^2 = h_{ik} dx^i dx^k \tag{26}$$

with the projection tensor

$$h_{ik} = g_{ik} + u_i u_k . \tag{27}$$

This means

$$ds^2 = d\sigma^2 - u_i u_k dx^i dx^k . \tag{28}$$

Note that $ds^2 = d\sigma^2$ for dx^i orthogonal to u^i , and $ds^2 = -d\tau^2$ for $dx^i = u^i d\tau$ (with τ being the proper time). $d\sigma^2$ can be used to measure infinitesimal proper distances on the disc. In the co-rotating frame where the four-velocity has only a fourth component (in the vicinity of the disc we consider a family of observers with the same property), we obtain

$$d\sigma^2 = h'_{\alpha\beta} dx'^{\alpha} dx'^{\beta} = \left(g'_{\alpha\beta} - \frac{g'_{\alpha 4} g'_{\beta 4}}{g'_{44}} \right) dx'^{\alpha} dx'^{\beta}, \quad \text{where } \alpha, \beta = 1, 2, 3. \tag{29}$$

Thus the line element $d\sigma^2$ corresponds to the result of the “radar method” of Landau and Lifschitz [14, § 84]. Since the projection tensor $h'_{\alpha\beta}$ does not depend on x'^4 in our case, we can also use it to calculate finite proper spatial distances via integration. This is due to the fact that the spacetime is stationary and the four-velocity field shares this symmetry. However, the four-velocity field is not hypersurface-orthogonal and the 3-space characterized globally by the line element (29) is not a hypersurface of spacetime.

From now on we are only interested in the proper spatial geometry of the disc itself, as a 2-dimensional object - described by the line element $d\sigma^2|_{\text{disc}} = \left\{ h'_{\alpha\beta} dx'^{\alpha} dx'^{\beta} \right\}|_{\text{disc}}$. This is the geometry observed by a family of “residents” of the disc who apply the radar method.

In elliptic coordinates the 2-dimensional proper spatial line element of the metric (6) takes the form

$$d\sigma^2|_{\nu=0} = f'^{-1} h' \rho_0^2 \frac{\eta^2}{1 - \eta^2} d\eta^2 + f'^{-1} \rho_0^2 (1 - \eta^2) d\varphi'^2. \tag{30}$$

Note that, since $\nu = 0$ on the disc, the elliptic coordinates decouple and $d\rho^2 = \rho_0^2 \frac{\eta^2}{1 - \eta^2} d\eta^2$ and $\rho^2 = \rho_0^2 (1 - \eta^2)$.

Integration of the line element (30) then gives the proper circumference

$$C'(\eta) = 2\pi\rho_0\sqrt{1 - \eta^2} f'^{-1/2}, \tag{31}$$

the proper area

$$A'(\eta) = 2\pi\rho_0^2 \int_{\eta}^1 d\tilde{\eta} \tilde{\eta} f'^{-1} h'^{1/2} \tag{32}$$

and the proper radius

$$R(\eta) = R'(\eta) = \rho_0 \int_{\eta}^1 d\tilde{\eta} \frac{\tilde{\eta}}{\sqrt{1 - \tilde{\eta}^2}} \left(f'^{-1} h' \right)^{1/2} \tag{33}$$

of the rotating disc of charged dust. By inserting the post-Newtonian expansions of the metric functions in the co-rotating frame, using (25), (24) and (9), also (31), (32) and (33) can be written as series expansions in g .⁴

⁴ When we state that the geometry is “seen” or “measured” by co-rotating observers, we actually mean that the co-rotating observers apply the radar method to measure distances. Since they are at rest relative to the rotating disc (and their four-velocity field, in accordance with the four-velocity field of fixed particles in the disc, has only a fourth component in the co-rotating frame), they measure the proper spatial geometry of the disc. In the non-rotating frame, on the other hand, the non-rotating observers also use the radar method. However, they are at rest relative to the non-rotating frame (with a four-velocity field that has vanishing spatial components in the non-rotating frame) and consequently do not measure the proper spatial geometry of the disc, but the proper spatial geometry of their own “rest space”.

Accordingly, in the non-rotating frame of reference circumference and radius are defined by $C(\eta) = 2\pi\rho_0\sqrt{1 - \eta^2} f^{-1/2}$ and $R(\eta) = \rho_0 \int_{\eta}^1 d\tilde{\eta} \frac{\tilde{\eta}}{\sqrt{1 - \tilde{\eta}^2}} \left(f^{-1} h \right)^{1/2}$, respectively.

In order to compare the results for C' , A' and R of the charged disc of dust with those of a standard disc within the framework of special relativity, described by Grøn, we have to take the Newtonian limit. Thus, we require that both the metric deviates only slightly from the Minkowski metric and the rotational velocities are small compared to the speed of light.

| | |
|---|--|
| <p>Charged disc of dust (Newtonian limit):</p> $C' = 2\pi\rho_0 \left[\rho^* + \left(\frac{1}{2}\Omega_1^{*2}\rho^{*2} - \frac{1}{2}f_2 \right) \rho^* g^2 \right],$ $A' = \pi\rho_0^2 \left[\rho^{*2} + \left(\frac{1}{4}\Omega_1^{*2}\rho^{*2} + \frac{1}{2}(2 - f_2) \right) \rho^{*2} g^2 \right],$ $R = \rho_0 \left[\rho^* + \frac{1}{6}(4 - f_2) \rho^* g^2 \right].$ | <p>Disc within SR (Newtonian limit):</p> $C' = 2\pi r \left[1 + \frac{1}{2}(\omega r)^2 \right],$ $A' = \pi r^2 \left[1 + \frac{1}{4}(\omega r)^2 \right],$ $R = r.$ |
|---|--|

Crucial to the discussion of Ehrenfest’s paradox and the closely related geometric questions is the ratio of circumference to radius as seen from co-rotating and non-rotating observers.

| | |
|---|--|
| <p>Charged disc of dust (Newtonian limit):</p> $\frac{C'}{R'} = 2\pi \left[1 + \left(\frac{1}{2}\Omega_1^{*2}\rho^{*2} - \frac{1}{3}(2 + f_2) \right) g^2 \right],$ $\frac{C}{R} = 2\pi \left[1 - \frac{1}{3}(2 + f_2) g^2 \right].$ | <p>Disc within SR (Newtonian limit):</p> $\frac{C'}{r} = 2\pi \left[1 + \frac{1}{2}(\omega r)^2 \right],$ $\frac{C}{r} = 2\pi.$ |
|---|--|

The first-order ($n = 1$) coefficient function f_2 is given by $f_2(\eta, 0) = -1 - \eta^2$ and $\rho^* = \frac{\rho}{\rho_0} = \sqrt{1 - \eta^2}$.

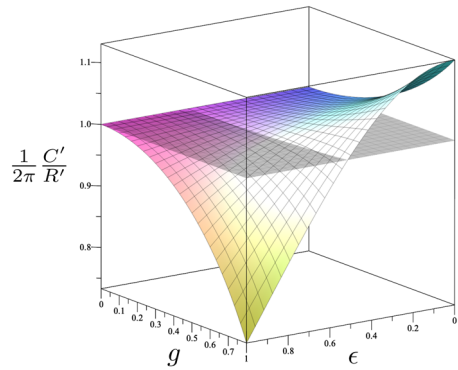
It should be noted that the above expansions utilize different expansion parameters and therefore only in the Newtonian limit a comparison is meaningful. For the disc of dust we demand the gravitational potential to be small compared to the speed of light c and the expansion parameter is $g = \frac{\sqrt{-U_c}}{c} \ll 1$. On the other hand, for the SR-disc we have expansions around small rotational velocities, $\frac{\omega r}{c} \ll 1$.

Grøn discusses only kinematic aspects of the disc and material properties are absent in [4, 12]. However, a real disc is hold together by attractive forces originating from the rigid material itself. In case of the disc of dust attractive gravitational forces, mediated through the terms involving f_2 , play the role of those material forces.

Taking the different expansions and the appearance of the terms with f_2 into account, the disc of dust agrees with Grøn’s investigated disc in the Newtonian limit.

Furthermore, an interesting observation can be made. The quantities C' , A' and R of the disc of dust are all larger than those of Grøn’s analysed disc (for $\eta^2 < 1$ and $r > 0$). Although dust is by definition a pressure-less fluid without any elastic properties, the rotating disc of dust nevertheless behaves to some extent as if it had material properties, resulting in a kind of “elastic” expansion.

Fig. 1 Normalized ratio of circumference to radius in the rotating frame plotted for $\eta = 0$



Explicitly writing out the ratios of circumference to radius leads to:

$$\frac{C'}{R'} = 2\pi \left[1 + \frac{1}{6} (1 - \eta^2) (1 - 3\epsilon^2) g^2 \right], \tag{34}$$

$$\frac{C}{R} = 2\pi \left[1 - \frac{1}{3} (1 - \eta^2) g^2 \right]. \tag{35}$$

Remarkably, for $\eta^2 < 1$, there is a geometrical transition induced by an alteration of the specific charge: $\frac{C'}{R'} \geq 2\pi$ for $\epsilon^2 \leq \frac{1}{3}$. This transition is also present beyond the Newtonian limit, as can be seen in Fig. 1. All figures in this paper are created using all available orders, i.e. up to $n = 10$. For vanishing charge the ratio of proper circumference to proper radius becomes larger than 2π , just as in the case of Grøn’s result for this ratio.

In the non-rotating frame there is no such transition, instead the ratio of circumference to radius is always smaller than 2π , independent of the specific charge (excluding $\eta = \pm 1$). This also stays true beyond the Newtonian limit (apart from high values of g), see Fig. 2. Within special relativity the ratio is exactly equal to 2π , as Grøn showed. Those results, however, do not contradict each other, since values smaller than 2π are caused by the gravitational correction term involving f_2 . As discussed above, Grøn’s analysis of the rotating disc does not involve corresponding terms.⁵

Now, let us address the questions raised in the beginning of this section, starting with the first one. Formulated in the Newtonian language, a dust particle in the rotating disc is in an equilibrium state of gravitational, electric and centrifugal force. It is therefore evident that changing the parameter ϵ directly affects the rotational velocity Ω . In particular, by decreasing ϵ we can transition to disc configurations with higher rotational velocities Ω . This, however, is achieved in a quasi-stationary way and cannot be seen as setting the disc into rotation as we alter the specific charge of the disc and

⁵ In the framework of special relativity there is an enlightening explanation for Grøn’s results: Observed in the non-rotating frame, not the circumference of the disc is being contracted due to rotation, but the infinitesimal measuring rods placed along the circumference. As a consequence observers on the rotating disc measure a ratio larger than 2π (they have to use more measuring rods), while an observer in the non-rotating frame still measures exactly 2π .

Fig. 2 Normalized ratio of circumference to radius in the non-rotating frame plotted for $\eta = 0$

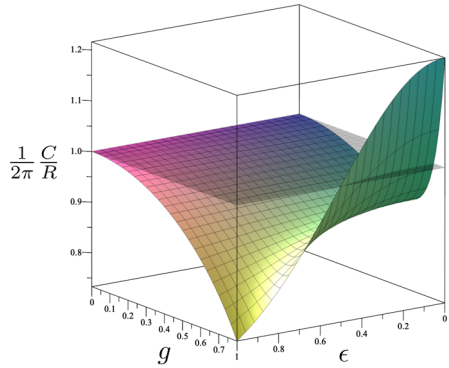
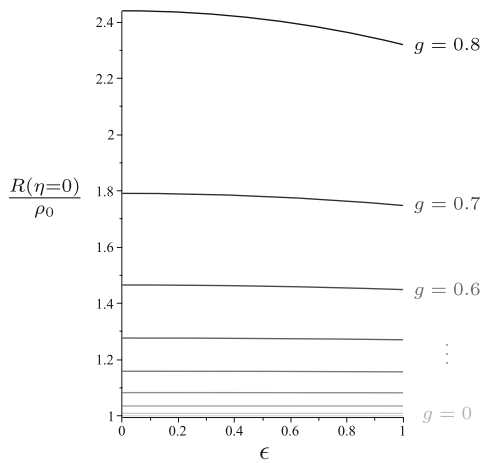


Fig. 3 Normalized proper radius, evaluated at the rim of the disc, as a function of ϵ



thus the disc itself. Nevertheless, we can compare disc configurations with increasing rotational velocities with each other and examine the effect on the spatial geometry. As can be seen in Fig. 1, for co-rotating observers the geometric ratio $\frac{C'}{R'}$ monotonically increases from values smaller to greater than 2π . In fact, as will be shown in Sect. 6, a simultaneous transition from positive to negative curvature also occurs. Non-rotating observers also measure increasing values of $\frac{C}{R}$. They, however, remain below 2π , apart from high values of g due to the emergence of an ergosphere.⁶

Concerning the second question, we have seen that the ratio $\frac{C'}{R'}$, that characterizes the proper spatial geometry and is measured by co-rotating observers, can be less than, equal to or greater than 2π depending on the specific charge ϵ . For a ratio equal to 2π the critical value of the specific charge is $\epsilon_{\text{crit}} = \frac{1}{\sqrt{3}}$ in the Newtonian limit. With growing g , ϵ_{crit} decreases slightly and becomes dependent on the radial coordinate η (see Figs. 15 and 16). Non-rotating observers, on the other hand, always perceive smaller values than 2π for $\frac{C}{R}$ (again, apart from high values of g).

⁶ We note that inside an ergosphere non-rotating (with respect to infinity) observers no longer exist.

Finally, the third question resolves around the influence of material properties present in a real rotating disc. Indeed, as we have already seen in the Newtonian limit, the disc of dust mimics “elastic” material properties and shows an “elastic” expansion as response to the rotational motion. But also beyond Newtonian physics, according to Fig. 3, the disc’s total proper radius $R_0 := R(\eta = 0)$ grows with decreasing specific charge ϵ and in turn increasing rotational velocities Ω . The more relativistic the disc, the more pronounced is the effect.

5 Curvature

Motivated by the found geometric transition induced by a change of the specific charge ϵ , we now examine the intrinsic curvature of rotating discs more closely.

As the domain of a rotating disc is simply a two-dimensional spatial surface, denoted by Σ_2 , the geometric quantity that describes its intrinsic curvature is the Gaussian curvature K .

In the following subsections we will calculate the Gaussian curvature of the charged rotating disc of dust (using the post-Newtonian expansion up to $n = 10$) and various analytic limiting cases. The findings will be compared and reviewed.

5.1 Gaussian curvature of the charged disc of dust

By using the derived expressions for the proper radius R and the proper circumference C' , (33) and (31), the proper spatial line element of the charged rotating disc of dust can be written in the following instructive and simple way:

$$d\sigma^2|_{\Sigma_2} = dR^2 + \left(\frac{C'(R)}{2\pi}\right)^2 d\varphi'^2, \tag{36}$$

where at least formally $C'(R) = C'(\eta(R))$.

With this condensed version of the proper spatial line element also the Gaussian curvature takes a very simply form, i.e.

$$K = -\frac{C'(R)_{,RR}}{C'(R)}. \tag{37}$$

It thus follows immediately that the Gaussian curvature of the charged rotating disc of dust is determined primarily by the second derivative of the proper circumference C' with respect to the proper radius R .

Even though the above formula for K , (37), is quite insightful, it is not that practical, since we do not know the functional dependence of C' on R . By using the chain rule we can, however, transform formula (37) into the slightly less appealing but all the more useful form

$$K = \frac{1}{C'(\eta)} \left(\frac{dR}{d\eta}\right)^{-3} \left[\frac{d^2R}{d\eta^2} C'(\eta)_{,\eta} - \frac{dR}{d\eta} C'(\eta)_{,\eta\eta} \right]. \tag{38}$$

Fig. 4 Gaussian Curvature K normalized by the total proper radius, R_0 , squared and evaluated at $\eta = 0$

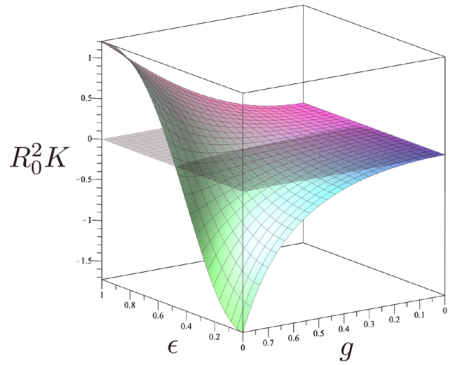
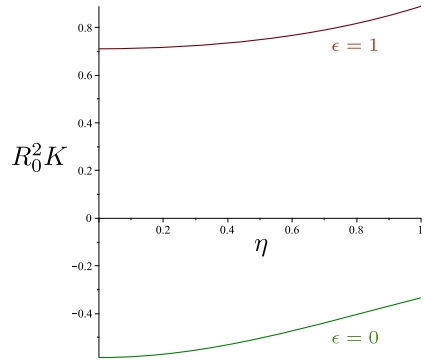


Fig. 5 Radial dependence of the normalized Gaussian curvature for the special cases $\epsilon = 0$ and $\epsilon = 1$, where $g = 0.6$



Inserting the solutions for the post-Newtonian expansion leads to

$$\begin{aligned}
 K = \frac{1}{\rho_0^2} & \left[(3\epsilon^2 - 1) g^2 \right. \\
 & + \left((6\eta^2 - 5) \epsilon^4 + \left(\frac{7}{6} - 8\eta^2 \right) \epsilon^2 + 3\eta^2 + \frac{1}{2} + \frac{16\eta^2}{\pi^2} (\epsilon^2 - 1) \right) g^4 \\
 & \left. + \mathcal{O}(g^6) \right]. \tag{39}
 \end{aligned}$$

As can be seen in Fig. 4, there is a characteristic transition curve in parameter space where the curvature K changes its sign. The same transition curve appears in Fig. 1 depicting $\frac{C'}{R'}$. Explicitly written out expansions up to fifth order of $\frac{C'}{R'}$ and $R_0^2 K$ are listed in appendix A.

Figure 5 shows the radial dependence of $R_0^2 K$ for the special cases $\epsilon = 1$ and $\epsilon = 0$. In case of maximal charge, i.e. $\epsilon = 1$, the disc has no rotation at all and general relativistic effects cause positive curvature. For $\epsilon = 0$ the rotation is maximal and special relativistic effects are dominant and lead, in accordance with the disc described by Grøn, to negative curvature. In both cases the curvature K gets more positive towards the centre of the disc (where $\eta = 1$). This is expected, since in the

Fig. 6 Functional dependence of C' (normalized by $2\pi R_0$) on R (normalized by R_0) plotted for $\epsilon = 0$ and $g = \{0, 0.2, 0.4, 0.6, 0.8\}$

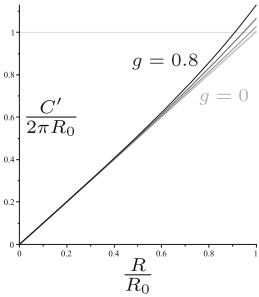


Fig. 7 Functional dependence of C' (normalized by $2\pi R_0$) on R (normalized by R_0) plotted for $\epsilon = 0.5$ and $g = \{0, 0.2, 0.4, 0.6, 0.8\}$

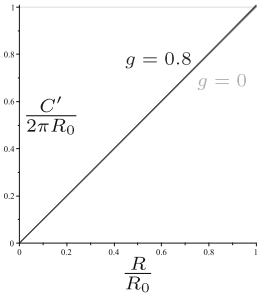
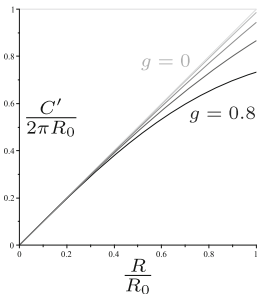


Fig. 8 Functional dependence of C' (normalized by $2\pi R_0$) on R (normalized by R_0) plotted for $\epsilon = 1$ and $g = \{0, 0.2, 0.4, 0.6, 0.8\}$



non-rotating case general relativistic effects increase towards the centre of a massive object, where the gravitational potential is the deepest. At maximal rotation, on the other hand, the rotational speed decreases towards the centre while general relativistic effects increase.

Interesting to the current discussion is also the functional dependence of C' on R that is visualized in terms of parametric plots (including appropriate normalizations) in Figs. 6, 7, 8. As can be observed there, $C'_{,RR} > 0$ for small ϵ and $C'_{,RR} < 0$ for large ϵ . Considering formula (37), this perfectly coincides with the plot of the normalized curvature in Fig. 4. The plots in Figs. 6, 7, 8 are also in line with the $\frac{C'}{R'}$ -plot in Fig. 1.

5.2 Newtonian theory: Maclaurin discs and their Gaussian curvature

In the Newtonian limit Einstein and Maxwell equations decouple and reduce to the Poisson equations for the gravitational and the electric potential. Thus, in Newtonian theory the disc of dust is fully described by

$$\Delta U = 4\pi\mu^{\text{Mld}}, \quad \text{with } \mu^{\text{Mld}} = \begin{cases} \sigma^{\text{Mld}}(\rho)\delta(\zeta) & \text{for } 0 \leq \rho \leq \rho_0 \\ 0 & \text{otherwise} \end{cases}, \quad (40)$$

$$\Delta U^{\text{E}} = -4\pi\epsilon\mu^{\text{Mld}}, \quad (41)$$

and

$$\epsilon U^{\text{E}}_{,\rho} = -\left(U - \frac{1}{2}\Omega^2\rho^2\right)_{,\rho}, \quad (42)$$

where U is the gravitational and $U^{\text{E}} := \alpha = -A_t$ the electric potential. Eq. (42) shows that the dust particles in the disc are in an equilibrium of electric, gravitational and centrifugal force.

Rotating discs in the framework of Newtonian theory characterized by (40)–(42) are also known as charged Maclaurin discs.

The solution for the exterior Newtonian gravitational potential of Maclaurin spheroids, in terms of elliptic coordinates, can be found in [10]. In the limit where the spheroid shrinks to a disc, this potential is given everywhere. As before, we are interested in the solution on the disc itself. On Σ_2 , where $\nu = 0$, the gravitational potential reduces to

$$U|_{\nu=0} = \frac{1}{2}U_c \left(1 + \eta^2\right), \quad (43)$$

with $U_c = -g^2$ in the Newtonian limit. According to Eqs. (40) and (41), U^{E} trivially follows from Eq. (43): $U^{\text{E}} = -\epsilon U$.

Furthermore, using the solution for U , (42) can be rewritten to the already known equation,

$$U_c = -\frac{\Omega^2\rho_0^2}{1 - \epsilon^2}, \quad (44)$$

that was used as a starting point for the post-Newtonian expansion.

Integrating (40) over an infinitesimal ζ -interval and exploiting reflection symmetry reveals the surface mass density

$$\sigma^{\text{Mld}} = \frac{1}{2\pi}U_{,\zeta}\Big|_{\zeta=0^+} = \frac{3M}{2\pi\rho_0^2}\eta, \quad (45)$$

where M is the mass of the disc. It can be easily verified that

$$U' = U - \frac{1}{2}\Omega^2\rho^2 \quad (46)$$

is the corotating potential in the Newtonian limit.

By understanding the Newtonian theory as a limit of the full general relativistic theory we can reuse the line element. The 4-dimensional line element in the Newtonian limit, evaluated on the disc, reads

$$\begin{aligned}
 ds^2 \Big|_{v=0} &= (1 - 2U) \rho_0^2 \frac{\eta^2}{1 - \eta^2} d\eta^2 + (1 - 2U) \rho_0^2 (1 - \eta^2) d\varphi'^2 \\
 &\quad + 2\Omega \rho_0^2 (1 - \eta^2) d\varphi' dt - (1 + 2U') dt^2.
 \end{aligned}
 \tag{47}$$

Using Eq. (29), the proper spatial line element of the Maclaurin disc follows immediately:

$$\begin{aligned}
 d\sigma^2 \Big|_{v=0} &= \left[1 + (1 + \eta^2) g^2 \right] \rho_0^2 \frac{\eta^2}{1 - \eta^2} d\eta^2 \\
 &\quad + \left[1 + (2 - \epsilon^2 (1 - \eta^2)) g^2 \right] \rho_0^2 (1 - \eta^2) d\varphi'^2.
 \end{aligned}
 \tag{48}$$

As expected, the Gaussian curvature of the Maclaurin disc resulting from (48) is given by:

$$K^{\text{Mld}} = \frac{1}{\rho_0^2} (3\epsilon^2 - 1) g^2.
 \tag{49}$$

In conclusion, the Gaussian curvature of the charged Maclaurin disc is in perfect agreement with the Gaussian curvature of the disc of dust in the Newtonian limit.

5.3 Gaussian curvature of a specific ECD-disc configuration

For general (not necessarily disc-) configurations with $\epsilon = \pm 1$ one obtains electrically counterpoised dust (ECD), see, e.g., [15]. Those solutions are static. The Papapetrou-Majumdar class [16, 17] contains such static solutions to the Einstein-Maxwell equations and the corresponding line element is of the form

$$ds^2 = f^{-1} \left[(d\rho^2 + d\zeta^2) + \rho^2 d\varphi^2 \right] - f dt^2,
 \tag{50}$$

where

$$f^{1/2} = e^U = 1 - \epsilon\alpha
 \tag{51}$$

is the defining relation between the metric function f and the electrostatic potential α . Due to the static spacetime the electromagnetic four-potential has only one non-vanishing component:

$$A_a = (0, 0, 0, -\alpha).
 \tag{52}$$

Starting from line element (50), the Einstein-Maxwell equations reduce to the surprisingly simple equation

$$\Delta e^{-U} = -4\pi \mu^{\text{ECD}} e^{-3U}.
 \tag{53}$$

By introducing a new potential V and a redefined mass density $\mu_{\text{st}}^{\text{ECD}}$ as

$$V := 1 - e^{-U} \quad \text{and} \quad \mu_{\text{st}}^{\text{ECD}} := \mu^{\text{ECD}} e^{-3U},
 \tag{54}$$

Eq. (53) can be transformed into the Poisson equation

$$\Delta V = 4\pi \mu_{st}^{ECD}. \tag{55}$$

The solution can consequently be represented as a Poisson integral and based on its asymptotic behaviour we can identify the mass:

$$M = \int \mu_{st}^{ECD}(\rho, \zeta) \rho \, d\rho \, d\varphi \, d\zeta. \tag{56}$$

For ECD the mass density μ_{st}^{ECD} is not predetermined by the theory, but can rather be freely chosen. As a physically motivated toy model, we consider a specific ECD-disc configuration equipped with the mass density of a Maclaurin disc:

$$\mu_{st}^{ECD} = \mu^{Mld}. \tag{57}$$

Note, that this means $\mu_{st}^{ECD} = e^{2U} \sigma_{st}^{ECD}(\rho) \delta(\zeta) = \sigma^{Mld}(\rho) \delta(\zeta)$. Choosing the mass density in this way is justified, since then the mass of the ECD-disc also coincides with the one of the Maclaurin disc: $M = \int \mu_{st}^{Mld}(\rho, \zeta) \rho \, d\rho \, d\varphi \, d\zeta = \int \mu_{st}^{Mld}(\rho, \zeta) \rho \, d\rho \, d\varphi \, d\zeta$.

In case of the Maclaurin disc, the equation of motion $\Delta U = 4\pi \mu^{Mld}$ leads to the solution $U|_{v=0} = \frac{1}{2} U_c (1 + \eta^2)$, see Eqs. (40) and (43). Analogously, for ECD the solution of (55) with the chosen mass density (57) is given by

$$V|_{v=0} = \frac{1}{2} V_c (1 + \eta^2). \tag{58}$$

However, now we get $V_c = -\frac{g^2}{1-g^2}$.

The proper spatial line element, stemming from (50), for the chosen ECD-disc configuration in terms of elliptic coordinates then reads

$$d\sigma^2|_{v=0} = f^{-1}|_{v=0} \left(\rho_0^2 \frac{\eta^2}{1-\eta^2} d\eta^2 + \rho_0^2 (1-\eta^2) d\varphi^2 \right), \tag{59}$$

where

$$f^{-1/2} = 1 - V, \quad V|_{v=0} = -\frac{1}{2} \frac{g^2}{1-g^2} (1 + \eta^2).$$

It implies the following Gaussian curvature:

$$K^{ECD} = \frac{1}{\rho_0^2} \frac{32 (1-g^2)^2 g^2}{[2 - (1-\eta^2) g^2]^4}. \tag{60}$$

The corresponding plot of the normalized Gaussian curvature can be found in Fig. 9. There we introduced $R_0^{ECD} := R^{ECD}(\eta = 0) = \rho_0 \frac{6-g^2}{6(1-g^2)}$.

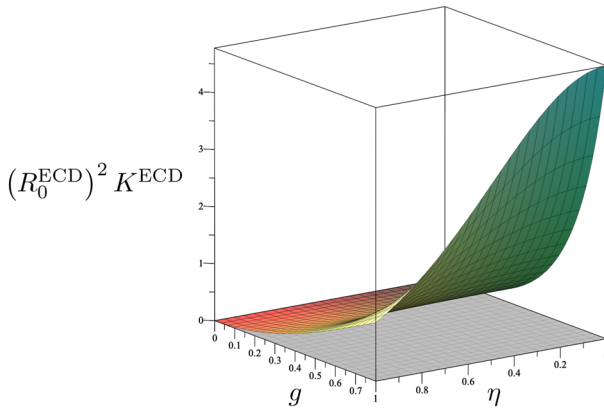


Fig. 9 Normalized Gaussian Curvature of the chosen ECD-configuration

Interestingly, in contrast to the charged rotating disc of dust (see Fig. 5), the chosen ECD-disc configuration possesses higher (positive) curvature at the rim of the disc and lower at the centre. But nevertheless, it has a positive curvature in agreement with the $\epsilon = 1$ -limit of the charged rotating disc of dust.

To gain a better understanding of this radial curvature behaviour, we investigate and compare the proper surface mass densities of the so far discussed discs. The resulting proper surface mass densities are

$$\begin{aligned} \sigma_p &= \sigma \sqrt{fh^{-1}} = \frac{1}{2\pi} U'_{,\zeta} \Big|_{\zeta=0^+} \sqrt{fh^{-1}} \\ &= \frac{2}{\pi^2 \rho_0} \left[\eta g^2 + \frac{1}{6} \left(\left(\frac{23}{3} \eta^2 - 5 \right) \epsilon^2 - 7\eta^2 \right) \eta g^4 + \mathcal{O}(g^6) \right], \end{aligned} \tag{61}$$

$$\begin{aligned} \sigma_p^{\text{Mld}} &= \sigma^{\text{Mld}} \\ &= \frac{2}{\pi^2 \rho_0} g^2 \eta, \end{aligned} \tag{62}$$

$$\begin{aligned} \sigma_p^{\text{ECD}} &= \sigma^{\text{ECD}} e^U \\ &= \frac{2}{\pi^2 \rho_0} \left[1 + \frac{1}{2} \frac{g^2}{1-g^2} (1+\eta^2) \right]^{-2} \frac{g^2}{1-g^2} \eta \\ &= \frac{2}{\pi^2 \rho_0} \left[\eta g^2 - \eta^3 g^4 + \mathcal{O}(g^6) \right]. \end{aligned} \tag{63}$$

As it should be, σ_p^{Mld} represents the Newtonian limit of σ_p and σ_p^{ECD} .

In Fig. 10 all three normalized proper surface mass densities are plotted and in Fig. 11 $R_0 \sigma_p|_{\epsilon=1}$ and $R_0^{\text{ECD}} \sigma_p^{\text{ECD}}$ are depicted for different values of the relativity parameter g .

From Fig. 11 it is evident that σ_p^{ECD} is denser at the rim and less dense at the centre compared to $\sigma_p|_{\epsilon=1}$. The higher g , the more extreme is this behaviour of the chosen ECD-configuration. This dominance of the proper surface mass density σ_p^{ECD} at the

Fig. 10 Comparison of the normalized proper surface mass densities $R_0^{\text{Mld}}\sigma_p^{\text{Mld}}$, $R_0\sigma_p$ and $R_0^{\text{ECD}}\sigma_p^{\text{ECD}}$ for $g = 0.7$ and $\epsilon = 1$

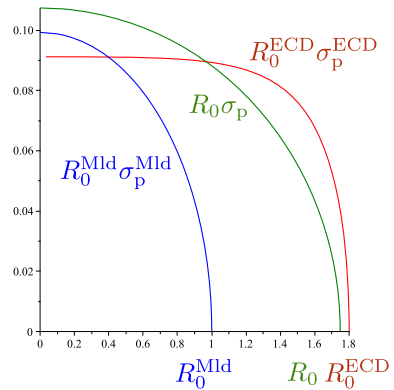
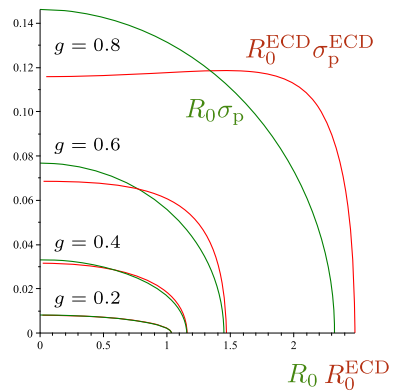


Fig. 11 Comparison of the normalized proper surface mass densities $R_0\sigma_p$ and $R_0^{\text{ECD}}\sigma_p^{\text{ECD}}$ for different values of g and $\epsilon = 1$



rim as opposed to the centre leads to the observed higher curvature K^{ECD} at the rim. In contrast, the curvature $K|_{\epsilon=1}$ generated by the surface mass density $\sigma_p|_{\epsilon=1}$ of the maximally charged disc of dust increases towards the centre.

5.4 Gaussian curvature of the uncharged disc of dust

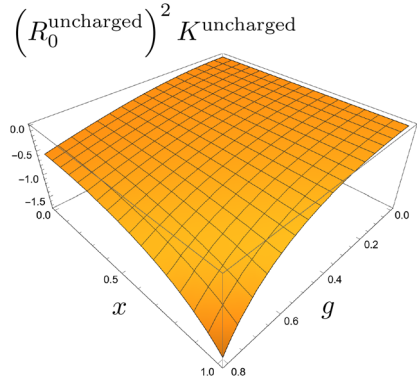
By means of the inverse scattering method that originates from soliton theory, the global problem of the uniformly rotating disc of dust without charge was solved rigorously by Neugebauer and Meinel [9, 10, 18].

An essential part of this method is to formulate and to solve a Riemann-Hilbert problem. It turns out that this Riemann-Hilbert problem has a unique solution in the parameter region $0 < \mu < \mu_0 := 4.629\dots$, where $\mu := 2(\rho_0\Omega)^2 e^{-2V_0}$ and $V_0 := U'(\rho = 0, \zeta = 0)$. $\mu \rightarrow 0$ corresponds to the Newtonian limit and for $\mu \rightarrow \mu_0$ the formation of a Kerr-black hole was proven [9, 18], see also [19].

Analogous to the charged disc, the line element can globally be written in Weyl-Lewis-Papapetrou form:

$$ds^2 = e^{-2U'} \left[e^{2k'} (d\rho^2 + d\zeta^2) + \rho^2 d\varphi'^2 \right] - e^{2U'} (dt + a d\varphi')^2. \quad (64)$$

Fig. 12 Normalized Gaussian curvature of the uncharged disc of dust



Denoting $x := \frac{\rho}{\rho_0}$, as used in the literature above, the resulting proper spatial line element reads

$$d\sigma^2|_{\Sigma_2} = e^{-2(U-k)} \rho_0^2 dx^2 + e^{-2V_0} \rho_0^2 x^2 d\varphi'^2, \tag{65}$$

utilising the boundary condition $e^{2U'} = e^{2V_0}$ and the transformation law $k' - U' = k - U$.

For the associated Gaussian curvature we obtain the compact formula

$$K^{\text{uncharged}} = -\frac{1}{2\rho_0^2 x} \frac{\partial}{\partial x} e^{2(U-k)} = -\frac{1}{2\rho_0^2 x} \frac{\partial}{\partial x} e^{2(V_0-k')}. \tag{66}$$

Hence the normalized Gaussian curvature plotted in Fig. 12 can be calculated by

$$\left(R_0^{\text{uncharged}}\right)^2 K^{\text{uncharged}}(g, x) = -2\mu k'_{,\tilde{\mu}}(\tilde{\mu}) \frac{\left[\int_0^1 dx e^{k'}(\tilde{\mu})\right]^2}{e^{2k'}(\tilde{\mu})}, \tag{67}$$

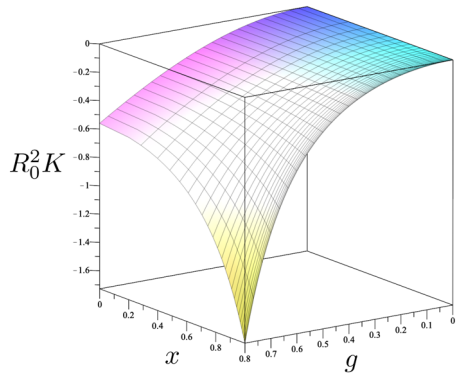
with $\tilde{\mu} := \mu(1 - x^2)$ and the relation $g(\mu) = \sqrt{1 - e^{V_0}(\mu)}$ between the parameters g and μ . The only occurring metric potential k' is related (within the disc) to the Ernst potential $e^{2V_0} + ib_0$ in the origin ($x = 0$) by

$$k'_{,\tilde{\mu}}(\tilde{\mu}) = \frac{1}{4} \frac{\left[e^{2V_0}_{,\tilde{\mu}}(\tilde{\mu})\right]^2 + \left[b_{0,\tilde{\mu}}(\tilde{\mu})\right]^2}{e^{2V_0}(\tilde{\mu})}. \tag{68}$$

These parameter functions e^{2V_0} and b_0 itself are given in terms of Jacobi’s elliptic functions.

Comparing the plot of the normalized Gaussian curvature of the uncharged disc (exact solution), Fig. 12, with the one of the charged disc evaluated at $\epsilon = 0$ (post-Newtonian expansion up to tenth order), Fig. 13, shows a good qualitative agreement.

Fig. 13 Normalized Gaussian curvature of the charged disc of dust in the limit of vanishing charge



Checking the more conclusive numerical values, certifies an excellent coincidence between the (exact) analytic and the semi-analytic solution for $\epsilon = 0$. Averaged over the disc (using $x = \{0, 0.3, 0.7, 1\}$), the percent deviation of $R_0^2 K|_{\epsilon=0}$ from $(R_0^{\text{uncharged}})^2 K^{\text{uncharged}}$ is 2.29×10^{-6} for $g = 0.6$, 3.50×10^{-5} for $g = 0.7$ and still only 4.72×10^{-4} for $g = 0.8$. See appendix B for the corresponding numerical values of the normalized Gaussian curvature.

5.5 Visualization

Similar to Flamm’s paraboloid in case of Schwarzschild spacetime, we want to visualize the spatial curvature of the charged disc of dust by an isometric embedding.

The isometric embedding of the proper 2-dimensional disc space, characterized by (36), into 3-dimensional Euclidean space, furnished with the line element $dl^2 = dr^2 + r^2 d\phi^2 + dz^2$ is achieved by the identifications

$$\phi = \phi', \tag{69}$$

$$r = \frac{C'(R)}{2\pi}, \tag{70}$$

$$z(R) = \int_0^R \left[1 - \frac{C'(\tilde{R})}{2\pi} \right]^{1/2} d\tilde{R}, \tag{71}$$

if the condition $C'(R),R \leq 2\pi$ is satisfied.

This means that this embedding only works for sufficiently high values of ϵ . Based on to the fact that the curvature becomes first negative at the centre of the disc by lowering ϵ (if initially it is positive everywhere), see Sect. 5.6, it can be shown that $K \geq 0$ is not only a sufficient but also a necessary condition for the embedding constraint, $C'(R),R \leq 2\pi$, to be fulfilled.

In Fig. 14 the embedding of the charged disc of dust is depicted for the values $g = 0.6$ and $\epsilon = 1$.

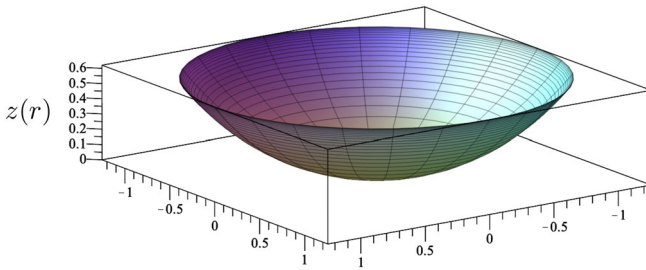
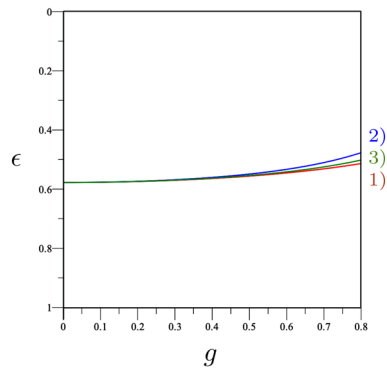


Fig. 14 Isometric embedding of the proper 2-dimensional disc space into 3-dimensional Euclidean space for $g = 0.6$ and $\epsilon = 1$. The scaling parameter ρ_0 is set to 1

Fig. 15 Conditions 1), 2), and 3) lead to the same transition curve in the parameter space. W.l.o.g. $\eta = 0$



5.6 Transition curve

In three different cases we have seen the occurrence of a transition curve in the parameter space (ϵ, g) :

$$1) \frac{C'}{R'} = 2\pi, \quad 2) K = 0, \quad 3) C'_{,R} = 2\pi.$$

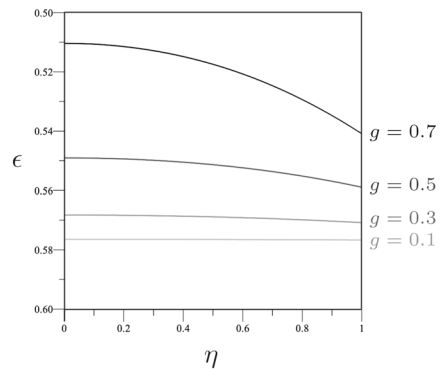
It turns out that all those three conditions are equivalent and indeed all the curves are identical. This is also backed up by Fig. 15.

The radial dependence of the transition curve can be read off from Fig. 16. As can be seen there, changing ϵ does not cause a transition throughout the whole disc at the same time. In fact, by starting with positive curvature, i.e. high values of ϵ , the transition to negative curvature happens first at the centre and last at the rim.

6 Discussion

A central assumption in cosmology is that the universe is spatially homogeneous and isotropic on large length scales. This is the cosmological principle and indeed observations confirm that it is fulfilled on scales of about 100 Mpc. Using the cosmo-

Fig. 16 Radial dependence of the curve $K = 0$ plotted for different values of the relativistic parameter g



logical principle one can straightforwardly derive the Friedmann-Robertson-Walker metric that reduces the Einstein equations to the famous Friedmann equations. Due to homogeneity and isotropy the solutions exhibit a globally constant geometry with only three possible spatial curvatures: flat ($k = 0$), positive ($k = +1$) or negative ($k = -1$). Remarkably, observations of the CMB suggest that our universe might indeed be flat. The first Friedmann equation reveals that there is a critical energy density that leads to a flat universe. If the density is higher than the critical density the universe is positively curved and if it is lower it is negatively curved. For more details see, e.g., [20].

In some sense the proper spatial geometry of the charged rotating disc of dust behaves analogous to the spatial curvature of the Friedmann universe. High values of the specific charge ϵ (defined as the ratio of electric charge to baryonic mass) cause positive and low values negative curvature. Furthermore, for given g and η there is a critical value of ϵ that gives rise to Euclidean geometry. However, unlike in Friedmann cosmology the geometry of the charged disc of dust is not globally constant. The geometry remains unchanged only in angular direction, but not in radial one. A beautiful exception of this represents the Newtonian limit with a radially independent curvature. In fact, for the critical value $\epsilon = \frac{1}{\sqrt{3}}$ the disc is globally flat.

Acknowledgements This work has been funded by the Deutsche Forschungsgemeinschaft (DFG) under Grant No. 406116891 within the Research Training Group RTG 2522/1. The authors would like to thank Martin Breithaupt for the provided results of the post-Newtonian expansion up to tenth order.

Funding Open Access funding enabled and organized by Projekt DEAL.

Data availability The datasets generated during and/or analysed during the current study are available from the corresponding author on reasonable request.

Declarations

Conflict of interest The authors have no relevant financial or non-financial interests to disclose.

Open Access This article is licensed under a Creative Commons Attribution 4.0 International License, which permits use, sharing, adaptation, distribution and reproduction in any medium or format, as long as you give appropriate credit to the original author(s) and the source, provide a link to the Creative Commons licence, and indicate if changes were made. The images or other third party material in this article are included in the article's Creative Commons licence, unless indicated otherwise in a credit line to the material. If

material is not included in the article’s Creative Commons licence and your intended use is not permitted by statutory regulation or exceeds the permitted use, you will need to obtain permission directly from the copyright holder. To view a copy of this licence, visit <http://creativecommons.org/licenses/by/4.0/>.

Appendix A Expansions up to fifth order

$$\begin{aligned}
 & \frac{1}{2\pi} \frac{C'}{R'} (\eta = 0) \\
 &= 1 - \frac{1}{2} \left(\epsilon^2 - \frac{1}{3} \right) g^2 + \frac{5}{24\pi^2} \left[\left(\epsilon^4 - \frac{52}{75} \epsilon^2 - \frac{53}{75} \right) \pi^2 - \frac{224\epsilon^2}{25} + \frac{224}{25} \right] g^4 \\
 & \quad - \frac{223}{1920\pi^2} \left[\left(\epsilon^6 - \frac{3457}{892} \epsilon^4 + \frac{113453}{112392} \epsilon^2 + \frac{31336}{14049} \right) \pi^2 \right. \\
 & \quad \left. - \frac{2560}{669} (\epsilon^2 - 1) \left(\epsilon^4 - \frac{313}{70} \epsilon^2 - \frac{257}{42} \right) \right] g^6 \\
 & \quad + \frac{3145}{48384\pi^4} \left[\left(\epsilon^8 - \frac{313007839}{40256000} \epsilon^6 + \frac{3055678201}{193228800} \epsilon^4 - \frac{6005877459}{644096000} \epsilon^2 - \frac{29078}{235875} \right) \pi^4 \right. \\
 & \quad \left. - \frac{111104}{15725} (\epsilon^2 - 1) \left(\epsilon^6 - \frac{69012347}{9374400} \epsilon^4 + \frac{113190529}{24998400} \epsilon^2 + \frac{78691}{13020} \right) \pi^2 \right. \\
 & \quad \left. + \frac{802816}{15725} (\epsilon^2 - 1)^2 \left(\epsilon^2 - \frac{15227}{1960} \right) \right] g^8 \\
 & \quad - \frac{2815391}{66355200\pi^4} \left[\left(\epsilon^{10} - \frac{379034234759}{41622740544} \epsilon^8 + \frac{95728571097211}{3874698756096} \epsilon^6 \right. \right. \\
 & \quad \left. \left. - \frac{103871864922476873}{2727787924291584} \epsilon^4 + \frac{14955289324645259}{495961440780288} \epsilon^2 - \frac{5355807104}{650355321} \right) \pi^4 \right. \\
 & \quad \left. - \frac{238424064}{19707737} (\epsilon^2 - 1) \left(\epsilon^8 - \frac{10000383870041}{1084307938560} \epsilon^6 + \frac{104207736848353}{5046960586752} \epsilon^4 \right. \right. \\
 & \quad \left. \left. - \frac{49539410937953809}{5921767088455680} \epsilon^2 - \frac{91863454}{13446279} \right) \pi^2 \right. \\
 & \quad \left. + \frac{78643200}{2815391} (\epsilon^2 - 1)^2 \left(\epsilon^6 - \frac{4169}{350} \epsilon^4 + \frac{6055401553}{271656000} \epsilon^2 + \frac{2656693}{46200} \right) \right] g^{10}
 \end{aligned}$$

$$\begin{aligned}
 & R_0^2 K (\eta = 0) \\
 &= (3\epsilon^2 - 1) g^2 - 5 \left(\epsilon^2 - \frac{7}{30} \right) (\epsilon^2 - 1) g^4 \\
 & \quad + \frac{1703}{320\pi^2} \left[\left(\epsilon^6 - \frac{52261}{20436} \epsilon^4 + \frac{219665}{122616} \epsilon^2 - \frac{3968}{15327} \right) \pi^2 - \frac{2560\epsilon^6}{5109} + \frac{34816\epsilon^4}{15327} \right. \\
 & \quad \left. - \frac{11776\epsilon^2}{5109} + \frac{8192}{15327} \right] g^6 \\
 & \quad - \frac{9769}{2016\pi^2} \left[\left(\epsilon^8 - \frac{274414949}{60020736} \epsilon^6 + \frac{119546257}{18756480} \epsilon^4 - \frac{249550409}{80027648} \epsilon^2 + \frac{16824}{48845} \right) \pi^2 \right. \\
 & \quad \left. - \frac{94976}{48845} \left(\epsilon^6 - \frac{964087}{142464} \epsilon^4 + \frac{1525885}{284928} \epsilon^2 - \frac{856}{1113} \right) (\epsilon^2 - 1) \right] g^8
 \end{aligned}$$

$$\begin{aligned}
 &+ \frac{316977977}{77414400\pi^4} \left[\left(-\frac{158969856}{316977977} + \epsilon^{10} - \frac{425179610969}{60859771584} \epsilon^8 + \frac{1000003956304379}{62320406102016} \epsilon^6 \right. \right. \\
 &- \frac{61149890345347447}{3988505990529024} \epsilon^4 + \frac{15274226506312301}{2659003993686016} \epsilon^2 \Big) \pi^4 - \frac{1296420864}{316977977} (\epsilon^2 - 1) (\epsilon^8 \\
 &- \frac{32218659817}{3646183680} \epsilon^6 + \frac{47760895613989}{2800269066240} \epsilon^4 - \frac{566746281193567}{59739073413120} \epsilon^2 + \frac{1129856}{949527} \Big) \pi^2 \\
 &\left. + \frac{550502400}{316977977} \left(\epsilon^4 - \frac{56}{5} \epsilon^2 + \frac{5296}{175} \right) (\epsilon^2 - 1)^2 \left(\epsilon^2 - \frac{1}{3} \right) \right] g^{10}
 \end{aligned}$$

Appendix B Gaussian curvature

Table 1 Gaussian curvature: uncharged disc (exact solution) versus charged disc in the limit $\epsilon \rightarrow 0$ (series expansion up to tenth order)

| | | $K^{\text{uncharged}} (R_0^{\text{uncharged}})^2$ | $K R_0^2 \Big _{\epsilon \rightarrow 0}$ |
|-----------|-----------|---|--|
| $g = 0.6$ | $x = 0$ | - 0.333602 | - 0.333602 |
| | $x = 0.3$ | - 0.349614 | - 0.349614 |
| | $x = 0.7$ | - 0.434073 | - 0.434072 |
| | $x = 1$ | - 0.584301 | - 0.584297 |
| $g = 0.7$ | $x = 0$ | - 0.441980 | - 0.441979 |
| | $x = 0.3$ | - 0.471784 | - 0.471784 |
| | $x = 0.7$ | - 0.640493 | - 0.640487 |
| | $x = 1$ | - 0.988126 | - 0.987999 |
| $g = 0.8$ | $x = 0$ | - 0.560113 | - 0.560108 |
| | $x = 0.3$ | - 0.611598 | - 0.611586 |
| | $x = 0.7$ | - 0.930419 | - 0.930281 |
| | $x = 1$ | - 1.73047 | - 1.72751 |

References

1. Ehrenfest, P.: Gleichförmige Rotation starrer Körper und Relativitätstheorie. *Physikalische Zeitschrift* **10**, 918 (1909)
2. Born, M.: Die Theorie des starren Elektrons in der Kinematik des Relativitätsprinzips. *Annalen der Physik* **335**, 1–56 (1909). <https://doi.org/10.1002/andp.19093351102>
3. Grøn, Ø.: In: Rizzi, G., Ruggiero, M.L. (eds.) *Space Geometry in Rotating Reference Frames: a Historical Appraisal*, pp. 285–333. Springer, Dordrecht (2004). https://doi.org/10.1007/978-94-017-0528-8_17
4. Grøn, Ø.: Relativistic description of a rotating disk. *Am. J. Phys.* **43**(10), 869–876 (1975). <https://doi.org/10.1119/1.9969>
5. Breithaupt, M., Liu, Y.-C., Meinel, R., Palenta, S.: On the black hole limit of rotating discs of charged dust. *Class. Quantum Gravity* **32**(13), 135022 (2015). <https://doi.org/10.1088/0264-9381/32/13/135022>

6. Palenta, S., Meinel, R.: Post-Newtonian expansion of a rigidly rotating disc of dust with a constant specific charge. *Class. Quantum Gravity* **30**(8), 085010 (2013). <https://doi.org/10.1088/0264-9381/30/8/085010>
7. Meinel, R., Breithaupt, M., Liu, Y.-C.: Black holes and quasiblack holes in Einstein-Maxwell theory. In: 13th Marcel Grossmann Meeting on Recent Developments in Theoretical and Experimental General Relativity, Astrophysics, and Relativistic Field Theories, pp. 1186–1188 (2015). https://doi.org/10.1142/9789814623995_0117
8. Ernst, F.J.: New formulation of the axially symmetric gravitational field problem. ii. *Phys. Rev.* **168**, 1415–1417 (1968). <https://doi.org/10.1103/PhysRev.168.1415>
9. Neugebauer, G., Meinel, R.: General relativistic gravitational field of a rigidly rotating disk of dust: solution in terms of ultraelliptic functions. *Phys. Rev. Lett.* **75**, 3046–3047 (1995). <https://doi.org/10.1103/PhysRevLett.75.3046>
10. Meinel, R., Ansorg, M., Kleinwächter, A., Neugebauer, G., Petroff, D.: Relativistic Figures of Equilibrium (2008). <https://doi.org/10.1017/CBO9780511535154>
11. Bardeen, J.M., Wagoner, R.V.: Relativistic disks I. Uniform rotation. *Astrophys. J.* **167**, 359–423 (1971)
12. Grøn, Ø.: Rotating frames in special relativity analyzed in light of a recent article by M. Strauss. *Int. J. Theor. Phys.* **16**(8), 603–614 (1977). <https://doi.org/10.1007/BF01811093>
13. Pirani, F.A.E., Williams, G.: Rigid motion in a gravitational field. *Séminaire Janet. Mécanique analytique et mécanique céleste* **5** (1961–1962). talk:8-9
14. Landau, L.D., Lifschitz, E.M.: *The Classical Theory of Fields*, (1971)
15. Meinel, R., Hütten, M.: On the black hole limit of electrically counterpoised dust configurations. *Class. Quantum Gravity* **28**(22), 225010 (2011). <https://doi.org/10.1088/0264-9381/28/22/225010>
16. Papapetrou, A.: A static solution of the equations of the gravitational field for an arbitrary charge-distribution. *Proceedings of the royal Irish academy. Sect. A: Math. Phys. Sci.* **51**, 191–204 (1945)
17. Majumdar, S.D.: A class of exact solutions of Einstein's field equations. *Phys. Rev.* **72**, 390–398 (1947). <https://doi.org/10.1103/PhysRev.72.390>
18. Neugebauer, G., Meinel, R.: The Einsteinian gravitational field of the rigidly rotating disk of dust. *Astrophys. J. Lett.* **414**, 97–99 (1993). <https://doi.org/10.1086/187005>
19. Meinel, R.: Black holes: a physical route to the Kerr metric. *Annalen der Physik* **514**, 509–521 (2002). <https://doi.org/10.1002/andp.20025140704>
20. Mukhanov, V.: *Physical Foundations of Cosmology* (2005). <https://doi.org/10.1017/CBO9780511790553>

Publisher's Note Springer Nature remains neutral with regard to jurisdictional claims in published maps and institutional affiliations.